IEEE Access
Multidisciplinary ⋮ Rapid Review ⋮ Open Access Journal

Received January 22, 2022, accepted February 7, 2022, date of publication February 10, 2022, date of current version February 17, 2022.

Digital Object Identifier 10.1109/ACCESS.2022.3150883

A New Reduced-Order Implementation of Discrete-Time Fractional-Order PID Controller

RAFAŁ STANISŁAWSKI[1], MAREK RYDEL[1], AND ZHIXIONG LI[2], (Senior Member, IEEE)
[1]Department of Electrical, Control and Computer Engineering, Opole University of Technology, 45-758 Opole, Poland
[2]Department of Manufacturing Engineering and Automation Products, Opole University of Technology, 45-758 Opole, Poland

Corresponding author: Rafał Stanisławski (r.stanislawski@po.edu.pl)

ABSTRACT This paper presents a new method for computationally effective implementation of a discrete-time fractional-order proportional–integral–derivative (FOPID) controller. The proposed method is based on a unique representation of the FOPID controller, where fractional properties are modeled by a specific finite impulse response (FIR) filter. The balanced truncation model order reduction method is applied in the proposed approach to obtain an effective, low-order model of the FOPID controller. The time-invariant FOPID controller implementation is presented first, and then the methodology is extended to the controller with time-varying gains. A comparative analysis shows that the proposed methodology leads to the effective modeling of discrete-time FOPID controllers. In addition to simulation runs, the effectiveness of the introduced methodology is confirmed in a real-life experiment involving the control of the DC motor servo system. The paper concludes with the implementation tools developed in the Matlab/Simulink environment.

INDEX TERMS Fractional-order discrete-time PID control, model order reduction, DC motor servo system.

I. INTRODUCTION

During the past two decades, the fractional-order generalizations of various control strategies have attracted considerable research attention in science and technology. A fractional-order proportional-integral-differential (FOPID) controller was first described in [1]. FOPID has two additional parameters compared to the classical PID controller, which are fractional orders of integrator and derivative. Moreover, since these extra parameters are mutually influenced by the controller's gains, tuning the parameters of the FOPID controller is much more challenging than for the classical integer-order case. To solve this problem, various optimization strategies have been applied, including particle swarm optimization [2]–[4], genetic algorithms [5], [6], differential evolution methods [5], chaotic firefly algorithms [7], extensions of classical tuning methods for PID controllers [8], [9], and other techniques [10]–[14]. Several implementations in control loops of various processes show that FOPID controllers can be effectively used, and their control performances can be much better than classical PID [14]–[23]. Additionally, the FOPID controllers can also apply fractional variable-order elements. However, the application of fractional-variable order is not unique and exists various solutions to this problem [24], [25]. Therefore, various variable-order FOPID controller implementations can be found in the literature [26]–[29].

A fundamental difficulty of the fractional-order element implementations is that the calculation of fractional-order integrator and derivative may lead to infinite complexity. Therefore, various approximations are used for the implementation of these elements. One of the most popular approaches in modeling the derivative/difference is the Oustaloup approximator. The Oustaloup method results in a rational, integer-order model described by the arbitrary order transfer function. This approximation convergence is quite high, requiring a relatively low model length to obtain satisfactory modeling performance in a given frequency range. The Oustaloup model has an elegant, simple form and can be easily calculated for both continuous- and discrete-time cases [4], [30]–[32]. Another popular approach is finite-length implementations of the Grünwald-Letnikov fractional-order integrator/derivative. In this case, the model is represented in the form of the discrete-time FIR (finite impulse response) filter. This conceptually simple method leads to high accuracy in the high-frequencies and can be easily implemented recursively. However, the main disadvantage of this FIR-based approach is a slow convergence of the algorithm. Similar to above, the FIR-class model

The associate editor coordinating the review of this manuscript and approving it for publication was Jiajie Fan.

results from power series expansion (PSE) applied to the Grünwald-Letnikov difference. Likewise, in the numerous papers [13], [32]–[34], we can find various discrete-time integer-order IIR-class filters, which can be obtained in many ways. These useful concepts use iterative algorithms such as continuous fraction expansion (CFE) and the Muir recursion based on the Tustin and Al-Alaoui discretization operators. An alternative IIR-based approach is the application of an orthonormal basis function-based model to the approximation of the Grünwald-Letnikov difference [35]. Comparative analysis of these approaches is presented in [32], [35]. Note that similar results may be obtained for Caputo and Riemann-Liouville definitions [36]–[38].

Considering all the above, to implement the FOPID controller, we have to use the fractional difference and integrator approximations. In the FOPID controllers, the finite-length implementations of the Grünwald-Letnikov fractional-order integrator/derivative, in terms or the Oustaloup approximations have often been used. For the first case, a high implementation length is required to obtain satisfactory accuracy in the low-frequency range, which leads to the high computational complexity of the FOPID model. Therefore, the accurate implementation of this approach is hardly realizable in real-time, especially in industrial platforms. A straightforward implementation of the discrete-time FOPID controller can be achieved for low implementation lengths of integrator/difference at the cost of accuracy (see, e.g., [18]). The second popular approach in FOPID controllers is based on the Oustaloup approximation. The Oustaloup approximation requires much lower model orders to obtain satisfactory modeling performances. Since the FOMCON toolbox for Matlab/Simulink [39] implements FOPID controllers using the Oustaloup approach, this method is the most commonly used in recent years [5], [9], [40]. Note that other Matlab/Simulink toolboxes for the implementation of fractional-order systems and controllers use the Oustaloup approximation (see e.g. FOTF toolbox [42], [43]). The outlook of the various implementation methods of FOPID controllers has been presented in [20], [42]. However, the steady-state error is one of the side effects of using classical approximations of the fractional-order elements within the FOPID controllers. It results that for $t \to \infty$, implementations of fractional-order integrator have no longer the integration property. In [6], [44] it is shown that using various optimization techniques reduces the steady-state error. Another way to eliminate steady-state error is proposed in [45], [46], where integer-order integration combined with fractional-order derivative is used to model the fractional-order integrator. In this case, for $t \to \infty$ the FOPID controller results in a classical PI controller, which eliminates the steady-state error of the closed-loop system. The main disadvantage of various discrete-time Oustaloup-based FOPID implementations is relatively low accuracy in the high-frequency range. This issue significantly decreases controller adequacy in the transient state, particularly for fast-dynamic systems.

In [47]–[49] it is shown that using model order reduction methods can be effective in approximation/ implementation of the fractional-order systems both in continuous-time and discrete-time cases. In particular, authors in [48] show a simple and effective method based on the balanced-truncation model reduction method applied to a specific FIR-based approximation of the discrete-time fractional-order system, the so-called FIRBT method. On this basis, we propose a new method for the implementation of the FOPID controller. It is based on a specific representation of the FOPID controller, with a FIR filter representing fractional-order elements. This enables implementing an analytically driven balanced truncation model order reduction method. As a result, we obtain an accurate approximation of the FOPID controller. Since the approach is based on the FIR-based model, the high-frequency accuracy of the FOPID approximation is provided. Additionally, we present a modification to the methodology for time-varying gains of the FOPID filter. In both cases, we obtain a low-order state-space model of the FOPID controller, which can be easily implemented in real-time applications on industrial computers of relatively low performance. Both methods are proposed for the discrete-time case, but they can be easily modified for continuous-time controllers. To evaluate the proposed implementation method's performance, we use the FOPID controller in the real-life experiment to control DC motor servo system [51].

This paper is organized as follows. Having introduced the problem of FOPID systems in Section I, the implementation/approximation problem formulation for FOPID controllers is presented in Section II. The main result in terms of a new implementation method for discrete-time FOPID controller is presented in Section III. In particular, we offer a) a specific form of state-space representation for FOPID controller, with the fractional properties modeled in a specific FIR filter, b) analytical implementation of balanced truncation model order reduction method to obtain a low and accurate approximation of FOPID controller, and c) modification to the approximation methodology for time-varying gains of the FOPID controllers. An analysis of the efficiency of the proposed methodology is compared to the Oustaloup-based methods for modeling FOPID controllers is presented in Section IV. Section V contains a real-life implementation of the FOPID controller in closed-loop control with the DC motor servo system. Conclusions of Section VI complete the paper.

II. PROBLEM FORMULATION

It is well known that the FOPID controller can be described as

$$u(t) = \left(K_p + K_i \mathcal{D}^{-\lambda} + K_d \mathcal{D}^{\mu}\right) e(t) \tag{1}$$

where t is the continuous time, K_p, K_i and K_d are the controller parameters, $e(t)$ and $u(t)$ are the controller input (error signal) and output (control signal), respectively, and $\mathcal{D}$ is the fractional-order derivation/integration operator.

Note that $\mathcal{D}^{-\lambda}$ denotes the integrator of fractional order $\lambda > 0$ and $\mathcal{D}^{\mu}$ denote the derivative of fractional order $\mu > 0$.

This paper considers a more useful, from the implementation point of view, a discrete-time equivalent of FOPID controller, defined in the uniform time scale $t \in \mathbb{T} = h\mathbb{Z} = \{0, h, 2h, \ldots\}$, $h \in \mathbb{R}_+$ (see [52], [53]). In this case, the fractional-order PID controller can be defined as follows

$$u(t) = \left(K_p + K_i\nabla^{-\lambda}(q) + K_d\nabla^{\mu}(q)\right)e(t) \tag{2}$$

where $e(t)$ and $u(t)$ are the system input and output, respectively, $\nabla^{-\lambda}(q)$ and $\nabla^{\mu}(q)$ denote the backward (nabla) discrete-time fractional-order integrator and difference, respectively, and q is the forward shift operator. The nabla fractional-order difference can be defined by the use of the discrete-time Grünwald-Letnikov operator as

$$\nabla^{\mu}e(t) = h^{-\mu}\sum_{j=0}^{t/h}(-1)^j\binom{\mu}{j}e(t-hj) = \nabla^{\mu}(q)e(t) \tag{3}$$

with $\nabla^{\mu}(q) = h^{-\mu}\sum_{j=0}^{t/h}(-1)^j\binom{\mu}{j}q^{-j}$. Note that the sum in Eq. (3) increases in every step of the simulation process, therefore in general form, the $\mathbb{Z}$-transform of the fractional-order difference is as

$$\nabla^{\mu}(z) = h^{-\mu}\sum_{j=0}^{\infty}(-1)^j\binom{\mu}{j}z^{-j} = h^{-\mu}(1-z^{-1})^{\mu}$$

Eq. (3) can still be used to calculate the fractional-order integrator $\nabla^{-\lambda}(q)$, with μ being substituted by $-\lambda$. Alternatively, the operator $\Delta^{-\lambda}(z)$ can also be obtained as follows

$$\nabla^{-\lambda}(z) = \frac{1}{\nabla^{\lambda}(z)} = \frac{1}{h^{-\lambda}\sum_{j=0}^{\infty}(-1)^j\binom{\lambda}{j}z^{-j}} \tag{4}$$

It is essential to note that, in general, the filters $\nabla^{-\lambda}(z)$ and $\nabla^{\mu}(z)$ cannot be implemented in practice due to the incorporation of the infinite sum, therefore in practical applications, their finite-length implementations can be employed in the form of

$$\nabla^{\mu}(z) \approx \nabla_L^{\mu}(z) = h^{-\mu}\sum_{j=0}^{L}(-1)^j\binom{\mu}{j}z^{-j} \tag{5}$$

$$\nabla^{-\lambda}(z) \approx \nabla_L^{-\lambda}(z) = \frac{1}{h^{-\lambda}\sum_{j=0}^{L}(-1)^j\binom{\lambda}{j}z^{-j}} \tag{6}$$

where L is the finite implementation length.

To obtain an accurate approximation of fractional-order difference and integrator, the value of L should be very high, in particular for low orders μ and λ, respectively. For example, to reach $||\nabla^{0.5}1(t) - \nabla_L^{0.5}1(t)||_{\infty} < 0.01$, we have to use $L > 2000$. Using high L can hardly be implementable in an industrial environment due to high computational complexity. Moreover, limit L of the fractional-order integrator in the FOPID controller leads to the control steady-state error (see e.q. [45], [46]). Solutions to these problems, related to computationally simple, accurate steady-state error-free modeling of the FOPID, are the paper's main contributions.

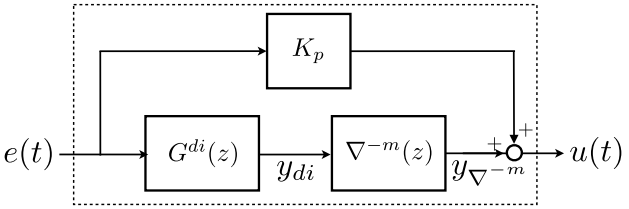

FIGURE 1. Block diagram of the discrete-time FOPID controller.

III. MAIN RESULTS

It is easy to show that the discrete-time FOPID controller of Eq. (2) can be presented in the form of

$$\begin{aligned} u(t) &= \left[\nabla^{-m}(q)\left(K_i\nabla^{m-\lambda}(q) + K_d\nabla^{m+\mu}(q)\right) + K_p\right]e(t) \\ &= \left[\nabla^{-m}(q)G^{di}(q) + K_p\right]e(t) \end{aligned} \tag{7}$$

where $G^{di}(q) = K_i\nabla^{m-\lambda}(q) + K_d\nabla^{m+\mu}(q)$, $\nabla^{-m}(q)$ is the discrete-time integer-order integrator, and $\nabla^{m-\lambda}(q)$ and $\nabla^{m+\mu}(q)$ are the fractional-order differences. The order $m \in \mathbb{Z}_+$ is selected as the ceiling function from the integrator order $m = \lceil\lambda\rceil$. The block diagram of the FOPID of Eq. (7) is presented in Fig. 1.

Fractional-order properties of the FOPID controller are described by the filter $G^{di}(q)$. Considering Eq. (5), the filter $G^{di}(q)$ can be approximated as

$$\begin{aligned} G^{di}(z) \approx G_L^{di}(z) &= K_i\nabla_L^{m-\lambda}(z) + K_d\nabla_L^{m+\mu}(z) \\ &= \sum_{j=0}^{L}(-1)^j\left[K_ih^{-m+\lambda}\binom{m-\lambda}{j}\right. \\ &\quad \left. + K_dh^{-m-\mu}\binom{m+\mu}{j}\right]z^{-j} \end{aligned}$$

Taking into account that the fractional-order differences $\nabla^{m-\lambda}(z)$ and $\nabla^{m+\mu}(z)$ (see Eq. (5)), and consequently the filter $G_L^{di}(z)$ are the class of an FIR model of order L, we have $G_L^{di}(q)\delta(t-t_0) = 0\ \forall\ t > t_0 + hL$, with $\delta(.)$ being the Kronecker delta. Therefore, for control error at the time t_0, the fractional-order PID responses as the discrete-time FOPID controller for $t \le t_0 + hL$, but for time $t > t_0 + hL$ the FOPID responses as integer-order PI controller. The above leads to the elimination of steady-state error, which is a well-known issue for the control process based on finite-memory FOPID controllers [45], [46].

The state space representation for the filter $G_L^{di}(z)$ is as

$$\begin{aligned} x(t+h) &= A_{G_L^{di}}x(t) + B_{G_L^{di}}e(t) \\ y_{di}(t) &= C_{G_L^{di}}x(t) + D_{G_L^{di}}e(t) \end{aligned} \tag{8}$$

where system matrices are as follows

$$A_{G_L^{di}} = \begin{bmatrix} 0 & 0 & \dots & 0 & 0 \\ 1 & 0 & \dots & 0 & 0 \\ 0 & 1 & \dots & 0 & 0 \\ \vdots & \vdots & \ddots & \vdots & \vdots \\ 0 & 0 & \dots & 1 & 0 \end{bmatrix} \tag{9}$$

$$B_{G_L^{di}} = \begin{bmatrix} 1 & 0_{1\times(L-1)} \end{bmatrix}^T \tag{10}$$

$$C_{G_L^{di}} = \begin{bmatrix} \phi_1 & \dots & \phi_L \end{bmatrix} \tag{11}$$

$$D_{G_L^{di}} = K_i h^{-m+\lambda} + K_d h^{-m-\mu} \tag{12}$$

where $A_{G_L^{di}} \in \Re^{L\times L}$, $B_{G_L^{di}} \in \Re^{L\times 1}$, $C_{G_L^{di}} \in \Re^{1\times L}$ and $D_{G_L^{di}} \in \Re$, with

$$\phi_j = K_i h^{-m+\lambda}(-1)^j \binom{m-\lambda}{j} + K_d h^{-m-\mu}(-1)^j \binom{m+\mu}{j} \tag{13}$$

$j = 1, \dots, L$ and $m = \lceil \lambda \rceil$.

In the discrete-time integer-order integrator $\nabla^{-m}(z)$ presented in the state space form

$$\begin{aligned} x(t+h) &= A_{\nabla^{-m}} x(t) + B_{\nabla^{-m}} y_{di}(t) \\ y_{\nabla^{-m}}(t) &= C_{\nabla^{-m}} x(t) + D_{\nabla^{-m}} y_{di}(t) \end{aligned} \tag{14}$$

we have

$$A_{\nabla^{-m}} = \begin{bmatrix} p_1(m) & p_2(m) & \dots & p_m(m) \\ 1 & 0 & \dots & 0 \\ 0 & 1 & \dots & 0 \\ 0 & 0 & \dots & 0 \end{bmatrix} \tag{15}$$

$$B_{\nabla^{-m}} = \begin{bmatrix} h^m & 0_{1\times(m-1)} \end{bmatrix}^T \tag{16}$$

$$C_{\nabla^{-m}} = \begin{bmatrix} p_1(m) & p_2(m) & \dots & p_m(m) \end{bmatrix} \tag{17}$$

$$D_{\nabla^{-m}} = h^m \tag{18}$$

where $p_i(m) = (-1)^{i+1}\binom{m}{i}$, $i = 1, \dots, m$.

Taking into account the block diagram of the FOPID shown in Fig. 1 we can finally present the model of the controller in the state space form

$$\begin{aligned} x(t+h) &= A_{PID} x(t) + B_{PID} e(t) \\ u(t) &= C_{PID} x(t) + D_{PID} e(t) \end{aligned} \tag{19}$$

with matrices $\{A_{PID}, B_{PID}, C_{PID}, D_{PID}\}$ as follows

$$A_{PID} = \begin{bmatrix} A_{G_L^{di}} & B_{G_L^{di}} C_{\nabla^{-m}} \\ 0_{m\times L} & A_{\nabla^{-m}} \end{bmatrix} = \begin{bmatrix} 0 & 0 & \dots & 0 & 0 & p_1(m) & p_2(m) & \dots & p_m(m) \\ 1 & 0 & \dots & 0 & 0 & 0 & 0 & \dots & 0 \\ 0 & 1 & \dots & 0 & 0 & 0 & 0 & \dots & 0 \\ \vdots & \vdots & \ddots & \vdots & \vdots & \vdots & \vdots & \vdots & \vdots \\ 0 & 0 & \dots & 1 & 0 & 0 & 0 & \dots & 0 \\ 0 & 0 & \dots & 0 & 0 & p_1(m) & p_2(m) & \dots & p_m(m) \\ 0 & 0 & \dots & 0 & 0 & 1 & 0 & \dots & 0 \\ 0 & 0 & \dots & 0 & 0 & 0 & 1 & \dots & 0 \\ 0 & 0 & \dots & 0 & 0 & 0 & 0 & \ddots & 0 \end{bmatrix} \tag{20}$$

$$\begin{aligned} B_{PID} &= \begin{bmatrix} B_{G_L^{di}} D_{\nabla^{-m}} & B_{\nabla^{-m}} \end{bmatrix}^T \\ &= \begin{bmatrix} h^m & 0_{1\times(L-1)} & h^m & 0_{1\times(m-1)} \end{bmatrix}^T \end{aligned} \tag{21}$$

$$\begin{aligned} C_{PID} &= \begin{bmatrix} C_{G_L^{di}} D_{G_L^{di}} C_{\nabla^{-m}} \end{bmatrix} \\ &= \begin{bmatrix} \phi_1 & \dots & \phi_L & \tilde{\phi}_1 & \dots & \tilde{\phi}_m \end{bmatrix} \end{aligned} \tag{22}$$

$$D_{PID} = D_{G_L^{di}} D_{\nabla^{-m}} + K_p = K_i h^{\lambda} + K_d h^{-\mu} + K_p \tag{23}$$

with ϕ_i, $i = 1, \dots, L$ and $p_i(m)$, $i = 1, \dots, m$, as in Eqs. (13) and (17), respectively, and elements $\tilde{\phi}_j \in \Re^{1\times 1}$, $j = 1, .., m$, calculated as

$$\tilde{\phi}_j = (K_i h^{-m+\lambda} + K_d h^{-m-\mu}) p_j(m) \tag{24}$$

Using the FIR filter $G_L^{di}(z)$ incorporated in the FOPID controller affects model complexity. To obtain satisfactory accuracy, we usually have to use $L > 1000$. Therefore, system with matrices dimensions $A_{PID} \in \Re^{(L+m)\times(L+m)}$, $B_{PID} \in \Re^{(L+m)\times 1}$, $C_{PID} \in \Re^{1\times(L+m)}$, and $D_{PID} \in \Re$ is hardly implementable in the industrial environment. To cope with the problem, we use model order reduction techniques to approximate $G_L^{di}(z)$ filter in the controller.

A. MODEL ORDER REDUCTION

This section applies the square root balanced truncation model order reduction method to model the filter $G_L^{di}(z)$. Consequently, we propose two approaches for modeling FOPID controllers with time-invariant parameters and time-varying gains.

1) TIME-INVARIANT CASE

The square root algorithm is based on the system's balanced form obtained using the singular value decomposition applied to the Cholesky factorizations of the controllability and observability matrices. Therefore, to construct the model, we have to determine the two factorizations, which are usually obtained as solutions of the Lyapunov equations. Solving these equations using numerical algorithms is the most time-consuming element in the whole model order reduction process. However, in [48] authors show that factorizations of the controllability and observability matrices for the fractional-order system $G_L^{di}(z)$ in the form of Eqs. (9)-(12) can be easily calculated analytically. Following the results of [48] we can propose the Cholesky factorizations of controllability and observability gramians S and R, respectively, in the form of

$$S = I_{L\times L} \tag{25}$$

$$R = \begin{bmatrix} \phi_L & 0 & 0 & \dots & 0 \\ \phi_{L-1} & \phi_L & 0 & \dots & 0 \\ \phi_{L-2} & \phi_{L-1} & \phi_L & \dots & 0 \\ \vdots & \vdots & \vdots & \ddots & \vdots \\ \phi_1 & \phi_2 & \phi_3 & \dots & \phi_L \end{bmatrix} \tag{26}$$

where ϕ_i, $i = 1, \dots, L$, are as in Eq. (11). The next step is calculating the SVD decomposition, which is the most time-consuming operation in the proposed method. Considering

that $S = I_{L\times L}$ we have

$$R^T = \begin{bmatrix} U_1 & U_2 \end{bmatrix} \begin{bmatrix} \Sigma_1 & 0 \\ 0 & \Sigma_2 \end{bmatrix} \begin{bmatrix} V_1 \\ V_2 \end{bmatrix} \tag{27}$$

where $\Sigma_1 = diag\,(\sigma_1, \cdots, \sigma_k)$, $\Sigma_2 = diag\,(\sigma_{k+1}, \cdots, \sigma_L)$, $\sigma_1 \geq \cdots \geq \sigma_k > \sigma_{k+1} \geq \cdots \geq \sigma_L > 0$, with σ_i, $i = 1, \ldots, L$ being the so called Hankel singular values. As it is presented in Eq. (27), the Hankel singular values can be divided into two parts $\Sigma_1 \in \mathbb{R}^{k\times k}$ and $\Sigma_2 \in \mathbb{R}^{(L-k)\times(L-k)}$. The order k is selected according to approximation accuracy of the reduced-order model, usually $k \ll L$. The transformation matrices used to obtain the reduced-order model are calculated using Petrov-Galerkin projections as

$$T = R^T V_1 \Sigma_1^{-0.5} = U_1 \Sigma_1^{0.5} \tag{28}$$

$$T^{\#} = S^T U_1 \Sigma_1^{-0.5} = U_1 \Sigma_1^{-0.5} \tag{29}$$

with $T^{\#}$ being the right inverse of the matrix T^T. Finally, we arrive at the model $\hat{G}_L^{di}(z)$ in form of (8) with the matrices as follows $\{T^T A_{G_L^{di}} T^{\#},\ T^T B_{G_L^{di}},\ C_{G_L^{di}} T^{\#},\ D_{G_L^{di}}\}$. It is worth emphasizing that model $G_L^{di}(z)$ is asymptotically stable due to the FIR structure (9)–(12). Thus using the balanced truncation method guarantees stability preservation of the model $\hat{G}_L^{di}(z)$.

Finally, we arrive to the FIRBT-based model of the fractional-order controller in form of (19), with the matrices as

$$A_{PID}^{BT} = \begin{bmatrix} T^T A_{G_L^{di}} T^{\#} & T^T B_{G_L^{di}} C_{\nabla^{-m}} \\ 0_{m\times k} & A_{\nabla^{-m}} \end{bmatrix} \tag{30}$$

$$B_{PID}^{BT} = \begin{bmatrix} T^T B_{G_L^{di}} D_{\nabla^{-m}} & B_{\nabla^{-m}} \end{bmatrix}^T \tag{31}$$

$$C_{PID}^{BT} = \begin{bmatrix} C_{G_L^{di}} T^{\#} & D_{G_L^{di}} C_{\nabla^{-m}} \end{bmatrix} \tag{32}$$

$$D_{PID}^{BT} = D_{PID} = K_i h^{\lambda} + K_d h^{-\mu} + K_p \tag{33}$$

where $A_{PID}^{BT} \in \mathbb{R}^{(k+m)\times(k+m)}$, $B_{PID}^{BT} \in \mathbb{R}^{(k+m)\times 1}$, $C_{PID}^{BT} \in \mathbb{R}^{1\times(k+m)}$ and $D_{PID}^{BT} \in \mathbb{R}$. Note that the final order of the FOPID controller is $k_{PID} = k + m$.

It is important to note that the approximation accuracy of the model (30)–(33) of the FOPID controller depends on the accuracy of the filter $\hat{G}_L^{di}(z)$. The filter $\hat{G}_L^{di}(z)$ is obtained by two approximation steps a) FIR-based approximation $G_L^{di}(z)$ and b) model order reduction of $G_L^{di}(z)$ to $\hat{G}_L^{di}(z)$, respectively. It is easy to show that the $\mathcal{H}_\infty$ norm of the modeling error for the $G_L^{di}(z)$ filter can be described by the equation

$$\begin{aligned} &||G^{di}(z) - G_L^{di}(z)||_{\mathcal{H}_\infty} \\ &= \sum_{j=0}^{L} (-1)^j \left[K_i h^{-m+\lambda} \binom{m-\lambda}{j} + K_d h^{-m-\mu} \binom{m+\mu}{j} \right] \end{aligned} \tag{34}$$

It is well known that $\mathcal{H}_\infty$ norm of the BT reduction satisfies the condition

$$||G_L^{di}(z) - \hat{G}_L^{di}(z)||_{\mathcal{H}_\infty} \leq 2 \sum_{j=k+1}^{L} \sigma_j \tag{35}$$

with $\sigma_j, j = 1, \ldots, L$, are as in Eq. (27). Combining Eqs. (34) and (35) we arrive at

$$\begin{aligned} ||G^{di}(z) - \hat{G}_L^{di}(z)||_{\mathcal{H}_\infty} \leq \sum_{j=0}^{L} (-1)^j \Bigg[& K_i h^{-m+\lambda} \binom{m-\lambda}{j} \\ & + K_d h^{-m-\mu} \binom{m+\mu}{j} \Bigg] + 2 \sum_{j=k+1}^{L} \sigma_j \end{aligned} \tag{36}$$

The actual convergence of the Hankel singular values is very rapid (see, e.g., [54]). Therefore, even for low order systems, the upper limit of Eq. (36) leads to satisfactory approximation.

Note that the above presented implementation method is realized only once for a given fractional-order PID controller. Every change of FOPID parameters leads to the re-implementation of the controller modeling procedure. In the next section, we present an alternative way of implementing FOPID controller for time-varying gains K_p, K_i, and K_d and still constant orders λ and μ.

2) TIME-VARYING CASE

In the case of modeling of fractional-order PID controller with time-varying parameters, we have to use the above methodology separately for modeling fractional-order discrete-time integrator and difference. The fractional-order integrator $\nabla^{-\lambda}(z)$ can still be modeled by the use of Eqs. (30)-(33), where $K_i = 1$, $K_p = 0$, and $K_d = 0$. On the other hand, the fractional-order difference $\nabla^{\mu}(z)$ can be modeled by $\hat{G}_L^{di}(z)$ in the form of (8) with the matrices as $\{T^T A_{G_L^{di}} T^{\#},\ T^T B_{G_L^{di}},\ C_{G_L^{di}} T^{\#},\ D_{G_L^{di}}\}$, with the parameters $K_i = 0$, $K_p = 0$, and $K_d = 1$. Therefore, finally, the matrices of the state-space model of fractional-order PID controller (19) are as

$$A_{TV-PID}^{BT} = \begin{bmatrix} T_d^T A_{\nabla_L^{\mu}} T_d^{\#} & 0_{k\times k} & 0_{k\times k} \\ 0_{k\times k} & T_i^T A_{\nabla_L^{m-\lambda}} T_i^{\#} & T_i^T B_{\nabla_L^{m-\lambda}} C_{\nabla^{-m}} \\ 0_{m\times k} & 0_{m\times k} & A_{\nabla^{-m}} \end{bmatrix} \tag{37}$$

$$B_{TV-PID}^{BT} = \begin{bmatrix} T_d^T B_{\nabla_L^{\mu}} & T_i^T B_{\nabla_L^{m-\lambda}} D_{\nabla^{-m}} & B_{\nabla^{-m}} \end{bmatrix}^T \tag{38}$$

$$C_{TV-PID}^{BT} = \begin{bmatrix} K_d C_{\nabla_L^{\mu}} T_d^{\#} & K_i C_{\nabla_L^{m-\lambda}} T_i^{\#} & K_i D_{\nabla_L^{m-\lambda}} C_{\nabla^{-m}} \end{bmatrix} \tag{39}$$

$$D_{TV-PID}^{BT} = D_{PID} = K_i h^{\lambda} + K_d h^{-\mu} + K_p \tag{40}$$

where $A_{\nabla_L^{\mu}} = A_{\nabla_L^{m-\lambda}} = A_{G_L^{di}}$, $B_{\nabla_L^{m-\lambda}} = B_{\nabla_L^{\mu}} = B_{G_L^{di}}$. The matrices $C_{\nabla_L^{\mu}} = C_{G_L^{di}}$, T_d and $T_d^{\#}$ are calculated using Eqs. (17), and (26)−(29), respectively, with $\phi_j = \phi_j^d = h^{-\mu} \sum_{k=1}^{j} (-1)^j \binom{\mu}{j}$, $j = 1, \ldots, L$. The matrices $C_{\nabla_L^{m-\lambda}} = C_{G_L^{di}}$, T_i and $T_i^{\#}$ are obtained in the same way with $\phi_j = \phi_j^i = h^{-m+\lambda} \sum_{k=1}^{j} (-1)^j \binom{m-\lambda}{j}$, $j = 1, \ldots, L$. Note that the order of time-varying FOPID controller of Eqs. (37)-(40) is $k_{TV-PID} = 2k + m$ and the orders of matrices are as follows $A_{TV-PID}^{BT} \in \mathbb{R}^{(2k+m)\times(2k+m)}$, $B_{TV-PID}^{BT} \in \mathbb{R}^{(2k+m)\times 1}$,

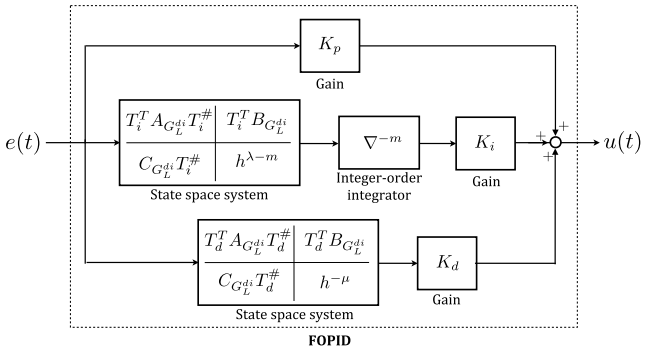

FIGURE 2. Block diagram of the time-varying discrete-time fractional-order PID controller.

$C^{BT}_{TV-PID} \in \mathbb{R}^{1\times(2k+m)}$ and $D^{BT}_{TV-PID} \in \mathbb{R}$. In the case of changing parameters K_p, K_i or K_d the most computationally burden process of selection of the balanced matrices T_i, $T_i^{\#}$, T_d and $T_d^{\#}$ is avoided, therefore only simple recalculation of C^{BT}_{TV-PID} and D^{BT}_{TV-PID} is required. Alternatively, the time-varying FOPID controller can be presented in an equivalent form using separate proportional, integral, and derivative parts. The block diagram of such representation is presented in Fig. 2.

The approximation accuracy for the time-varying FOPID can be analyzed in a similar way to the time-invariant FOPID. It is important to note that the final order of the time-varying FIRBT-based FOPID controller is $k_{TV-PID} = 2k + m$. Therefore, to obtain comparable approximation accuracy, we have to use higher order of the FOPID approximation. In the specific cases of fractional-order PI (FOPI) and fractional-order PD (FOPD) controllers, the time-varying models of the controllers are equivalent to the time-invariant models.

B. ALGORITHMS

The sampling period h of the FOPID controller has to be selected with regard to the upper bound of the frequency-domain characteristic of the controller. The approximation length L has to be selected according to the lower bound of the adequacy range of the FOPID controller. Assuming the number of decades of adequacy range is $\overline{w}$, then approximation length is $L = 10^{\overline{w}}$. Finally, the model's frequency adequacy range is $\omega \in \left[\frac{\pi}{Lh}, \frac{\pi}{h}\right]$ rad/s. Note that the proposed implementation methodology in both time-invariant and time-varying cases uses a numerically involving and memory-consuming SVD method, which leads to a high computational burden, particularly for implementation length $L > 10000$. Therefore, using $\overline{w} \leq 4$ is recommenced.

Based on the results presented above, we propose the following algorithms to generate two versions of the FOPID controller.

1) TIME-INVARIANT CASE

Input FOPID parameters: gains K_i, K_p, K_d, fractional orders λ, μ, sampling period h, approximation length L, the order k of the model $\hat{G}^{di}_L(z)$.

1) Calculate Cholesky factorization of the observability gramian R on the basis on Eq. (26)
2) Calculate transformation matrices T and $T^{\#}$ as in Eqs. (28) and (29)
3) Calculate the FIRBT-based FOPID controller as in Eqs. (30)-(33)

2) TIME-VARYING CASE

Input FOPID parameters: gains K_i, K_p, K_d, fractional orders λ, μ, sampling period h, approximation length L, the order k of the models ∇_L^{μ} and $\nabla_L^{-\lambda}$

1) Calculate transformation matrices T_i, $T_i^{\#}$, T_d and $T_d^{\#}$ as is presented in Section III-A2
2) Calculate the FOPID model matrices A^{BT}_{TV-PID} and B^{BT}_{TV-PID} as in Eqs. (37) and (38)
3) Each time step: Calculate C^{BT}_{TV-PID} and D^{BT}_{TV-PID} for current values of K_i, K_p, K_d as in Eqs. (39) and (40).

As a result of the above algorithms, we obtain an approximation of the FOPID controller in the form of the discrete-time state-space system of order k_{PID} or k_{FV-PID}. Considering that computational complexity of one-step control signal calculation is the class of $\mathcal{O}^2$ and k_{PID} and k_{TV-PID} is relatively low, therefore the real-time control can easily be applied in most of the industrial microcontrollers. Note that the time-invariant FOPID implementation requires all parameters, i.e., K_p, K_i, K_d, λ and μ constant. Changing any of the parameters' values involves recalculation of the algorithm, which is unimplementable in real-time. For the time-varying approach, the controller gains K_p, K_i, K_d can be changed in real time without recalculating the FOPID controller. However, λ and μ still have to be constant.

Appendix I presents the implementation tool for the fractional-order PID controller in the Matlab/Simulink environment based on the presented algorithms.

IV. EFFICIENCY ANALYSIS

In this section, the models of both FOPI and FOPID controllers are analyzed in the time and frequency domains. The parameters of FOPI and FOPID controllers, such as K_i, K_p, K_d, λ, and μ, are tuned for the DC motor system according to [41]. The modeling performance of the methodology presented in the paper is compared to the various Oustaloup approximations [30], [39], Tustin approach using CFE method, and PSE-based Euler approximation [32], [35].

A. FOPI CONTROLLER

Consider the FOPI controller with its parameters as follows: $K_p = 5.4972\text{e-}2$, $K_i = 5.5043\text{e-}2$, $\lambda = 0.6631$ as in [41]. Assuming the adequacy range of the FIRBT-based FOPI controller is $\omega \in [0.01\pi, 100\pi]$ rad/s, thus $h = 0.01$ s and $L = 10000$. The FIRBT-based controller is modeled using Eqs. (30)−(33) with $k = 3, 5, 7, 9$ and 11, which results in the following FOPI model lengths $k_{PI} = k + m = 4, 6, 8, 10$ and 12, respectively. These models are compared to the FOPI controllers based on:

TABLE 1. Norm of errors of models' impulse responses.

Order	Oustaloup		Modified Oustaloup		Tustin CFE		Euler PSE		FIRBT	
	$\|\|.\|\|_2$	$\|\|.\|\|_\infty$	$\|\|.\|\|_2$	$\|\|.\|\|_\infty$	$\|\|.\|\|_2$	$\|\|.\|\|_\infty$	$\|\|.\|\|_2$	$\|\|.\|\|_\infty$	$\|\|.\|\|_2$	$\|\|.\|\|_\infty$
$k_{PI}=4$	0.3033	0.2597	–	–	1.3584	0.0957	0.1117	0.0556	1.4502	1.7703e-02
$k_{PI}=6$	0.2654	0.2597	0.3043	0.2597	1.3159	0.0957	0.0771	0.0104	0.1248	2.5159e-03
$k_{PI}=8$	0.2666	0.2597	0.2894	0.2597	1.2765	0.0957	0.0760	4.3015e-03	7.9188e-03	2.4543e-04
$k_{PI}=10$	0.2733	0.2597	0.2888	0.2597	1.2391	0.0957	0.0760	2.3181e-03	3.2126e-03	1.0660e-04
$k_{PI}=12$	0.2793	0.2597	0.2885	0.2597	1.2031	0.0957	0.0758	1.8594e-03	1.7718e-03	7.0124e-05

- the Osutaloup approximation of orders $N = 1, \ldots, 5$, which results in the FOPI model lengths $k_{PI} = 2N + 2$, and optimized frequency adequacy range $\omega \in [\omega_b, \omega_h]$.
- the modified Oustaloup approximation of orders $N = 1, \ldots, 4$, which results in the FOPI model lengths $k_{PI} = 2N + 4$, and optimized frequency adequacy range $\omega \in [\omega_b, \omega_h]$ (see Section 12.1.3 in [30]).
- the Tustin-CFE approximations, which results in the respective FOPI model lengths k_{PI}.
- the Euler-PSE approximation with implementation length 10000 and application of BTA reduction algorithm resulting in the respective FOPI model lengths k_{PI}.

Analyses consider discretized Oustaloup-based models with the sampling period $h = 0.01$ s. The frequency responses and approximation errors of the considered model compared to the actual FOPI controller are presented in Figs. 3–4. The errors of frequency responses in Figs. 3–4 are calculated as

$$20 \log |G_{PID}(e^{j\omega h}) - \hat{G}_{PID}(e^{j\omega h})|$$

where $G_{PID}(e^{j\omega h})$ and $\hat{G}_{PID}(e^{j\omega h})$ are frequency responses of the actual and approximated FOPID controllers, respectively.

It can be seen from Figs. 3−4 that for the high- and medium-frequency ranges, the FIRBT-based FOPID controllers lead to lower approximation errors than the both Oustaloup-based models of respective orders. In contrast, in the low-frequency ranges, the Oustaloup-based models produce lower approximation errors than the FIRBT-based approach. Overall, higher order FIRBT-based models of the FOPI controller outperform Oustaloup-based implementations in the majority of the given adequacy range. Moreover, the Oustaloup-based implementation may lead to instability due to some numerical problems [55]. Note that the discrete-time version of the Modified Oustaloup approach generates similar results to the regular Oustaloup method. The Tustin-CFE-based models give unsatisfactory results regardless of the model orders. The Euler-PSE approximation produces comparable results to our FIRBT-based approach. However, the model calculation is a much more time-consuming process compared to our approach, due to the necessity of solving the Lyapunov equations.

As it is presented in Subsection III-B, the selection of the model in the adequacy range $\overline{w} \geq 4$ leads to the time-consuming implementation process. In contrast, both Oustaloup-based approximations is computationally simple regardless of the chosen frequency range. However, their

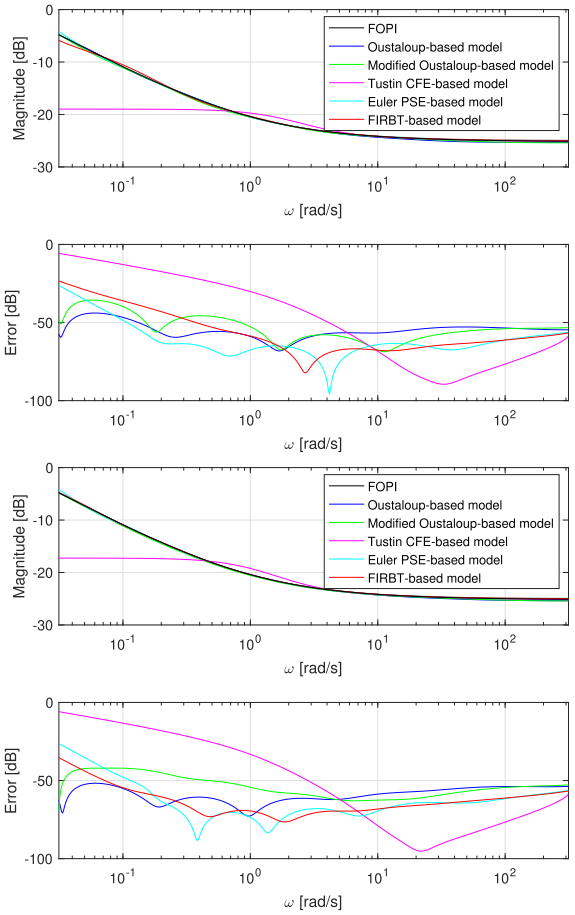

FIGURE 3. Frequency responses and approximation errors of various approximations of the FOPI controller for $k_{PI} = 6$ (up), and $k_{PI} = 8$ (down).

main drawback is low accuracy for high frequencies, which can be observed in Figs 3−4. L_∞ and L_2 norms of the impulse response errors of all considered FOPI controller approximations for $t \in [0, 10]$ s are presented in Table 1. Fig. 5 presents the impulse responses and approximation errors for considered FOPI models for $k_{PI} = 6$.

It can be seen from Table 1 that the proposed in the paper controller implementation methodology leads to effective time-domain approximation for $k_{PI} \geq 6$. Moreover, increasing the model orders significantly reduces the approximation errors. This high approximation effectiveness is mainly due to the time-domain nature of the proposed methodology, which results in the model's high-frequency accuracy.

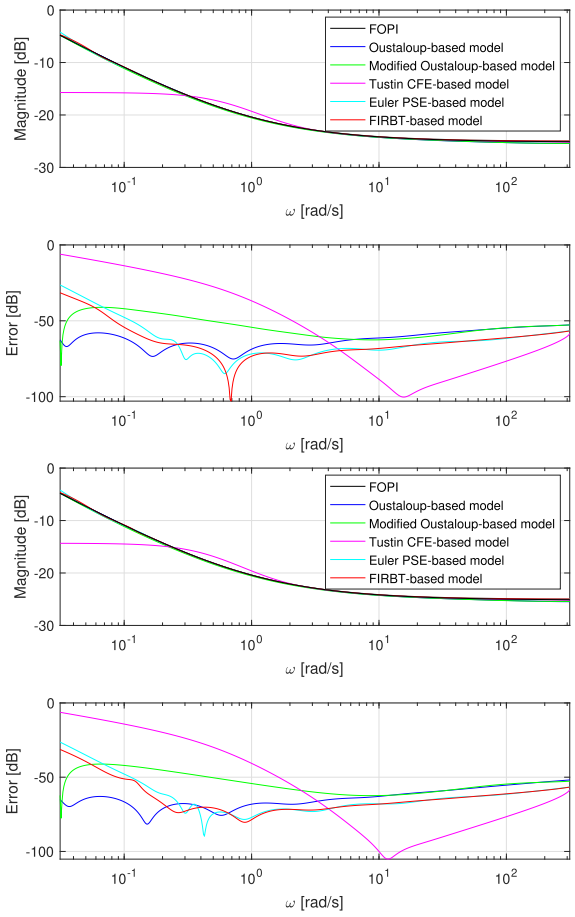

FIGURE 4. Frequency responses and approximation errors of various approximations of FOPI controller for $k_{PI} = 10$ (up), and $k_{PI} = 12$ (down).

Moreover, note that increasing Oustaloup approximations implementation length does not increase modeling accuracy in the time domain. It is a result of the inadequate high-frequency accuracy of the both Oustaloup approaches. It is not surprising that the Tustin-CFE approximation gives the least accurate results. It is a result of specific time-domain properties of the model [35]. The Euler-PSE approach generates comparable results to our FIRBT-based model, particularly for low approximation orders, where even better results can be obtained.

B. FOPID CONTROLLER

Consider the FOPID controller with its parameters as follows: $K_p = 0.005$, $K_i = 0.021235$, $K_d = 0.0014588$, $\lambda = 0.8$ and $\mu = 0.5$ as in [41]. As for the FOPI case, assume the adequacy range of the FIRBT-based FOPID controller as $\omega \in [0.01\pi, 100\pi]$ rad/s, therefore $h = 0.01$ s and $L = 10000$. The FIRBT-based FOPID controller is implemented using the time-invariant model of Eqs. (30)−(33) and the time-varying model of Eqs. (37)−(40). As in the case of FOPI, the obtained models are compared to the FOPID controllers based on the Oustaloup and modified Oustaloup approximations as well as Tustin-CFE, and Euler-PSE approaches. All FOPID approximations have the same orders

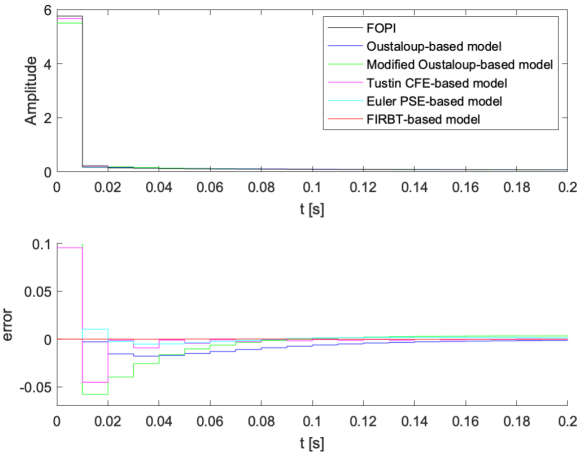

FIGURE 5. Impulse responses and approximation errors of various approximations of FOPI controller for $k_{PI} = 6$.

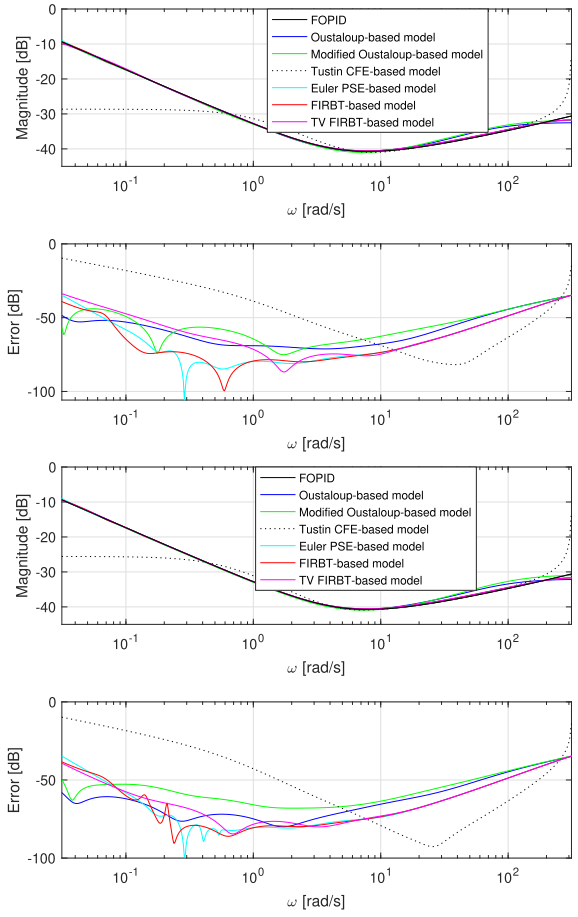

FIGURE 6. Frequency responses and approximation errors of various approximations of FOPID controller for $k_{PID} = 11$ (up), and $k_{PID} = 15$ (down).

$k_{PID} = 7,\ 11,\ 15,\ 19$ and 23. The frequency responses and approximation errors of the considered models compared to the actual FOPID controller are presented in Figs 6−7.

It can be seen from Figs. 6 and 7 that the general remarks for FOPI case are the same as for the FOPID controllers. The FIRBT-based models of the FOPID controller give overall

TABLE 2. Norm of errors of models' impulse responses.

Order	Oustaloup		Modified Oustaloup		Tustin CFE		Euler PSE		FIRBT		TV FIRBT	
	$\|\|.\|\|_2$	$\|\|.\|\|_\infty$	$\|\|.\|\|_2$	$\|\|.\|\|_\infty$	$\|\|.\|\|_2$	$\|\|.\|\|_\infty$	$\|\|.\|\|_2$	$\|\|.\|\|_\infty$	$\|\|.\|\|_2$	$\|\|.\|\|_\infty$	$\|\|.\|\|_2$	$\|\|.\|\|_\infty$
$k_{PID} = 7$	0.5154	0.4329	–	–	2.9775	1.3273	0.0275	3.1534e-03	0.0207	4.6828e-04	0.2969	4.8733e-03
$k_{PID} = 11$	0.2364	0.1906	0.2392	0.1371	3.3515	1.3273	0.0269	7.1671e-04	1.1860e-03	5.5237e-05	0.0185	7.1685e-04
$k_{PID} = 15$	0.2002	0.1313	0.3323	0.2717	3.5869	1.3273	0.0269	7.1596e-04	4.4988e-04	2.9623e-05	5.1718e-03	1.3417e-04
$k_{PID} = 19$	0.1898	0.1175	0.3544	0.2921	3.7559	1.3273	0.0268	7.1590e-04	3.2379e-04	2.3097e-05	1.9420e-03	5.9883e-05
$k_{PID} = 23$	0.1839	0.1115	0.3638	0.2995	3.8863	1.3273	0.0268	7.1590e-04	2.7702e-04	2.0109e-05	9.9176e-04	5.2108e-05

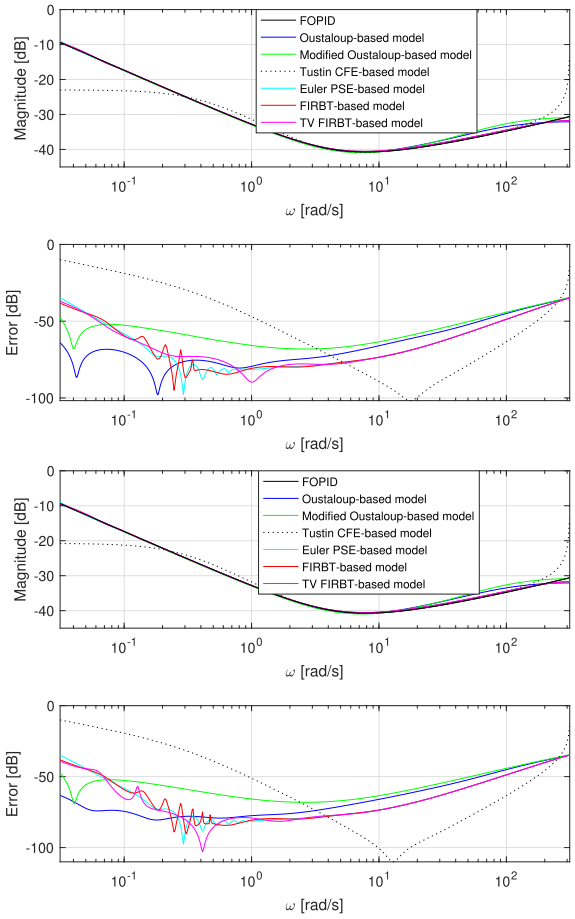

FIGURE 7. Frequency responses and approximation errors of various approximations of FOPID controller for $k_{PID} = 19$ (up), and $k_{PID} = 23$ (down).

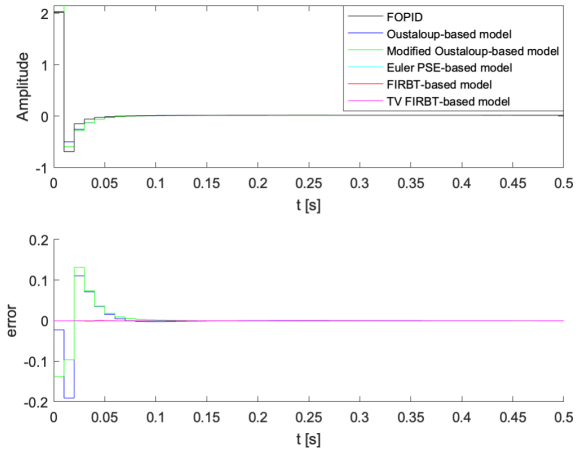

FIGURE 8. Impulse responses and approximation errors of various approximations of FOPID controller for $k_{PID} = 11$.

better approximation performance than both Oustaloup-based implementations for the majority of the chosen adequacy range. Oustaloup-based FOPID approximations may generate a lower approximation error than the FIRBT-based models for the low-frequency range only. Again, the Tustin-CFE-based model gives unsatisfactory accuracy, and the Euler-PSE approximation generates comparable results to our FIRBT-based approach, however, at the cost of a very time-consuming reduction process. Note that the time-varying FIRBT-based model also gives satisfactory accuracy. However, we have to use higher controller order to obtain equivalent accuracy to the time-invariant case. It is a cost of using the BT method separately for fractional-order integrator and derivative, respectively.

Again, in the analysis we have discretized the both Oustaloup-based models with the sampling period $h = 0.01$ s. L_∞ and L_2 norms of the impulse response errors for all considered models of the FOPID controller for $t \in [0, 10]$ s are presented in Table 2. Fig. 8 presents the impulse response and approximation errors for considered FOPID models for $k_{PID} = 11$.

It can be seen in Table 2 that the introduced implementation methodology leads to a more effective approximation of the FOPID filter than all considered methods. The only Euler-PSE method gives comparable accuracy to FIRBT and TV-FIRBT results. Moreover, again the Oustaloup-based implementations can lead to the instability of the FOPID filter.

V. IMPLEMENTATION TO THE DC MOTOR SERVO SYSTEM

In this section, the introduced methodology has been applied to control a DC motor for the INTECO modular servo system [51], [56]. Various FOPID implementation and optimization techniques have been considered on this platform in [41], [57]–[59]. This experimental platform consists of six components in terms of a 24 V DC motor, an inertia load, a magnetic brake, an encoder, a tachogenerator, and a gearbox. The servo system is connected to a PC through a

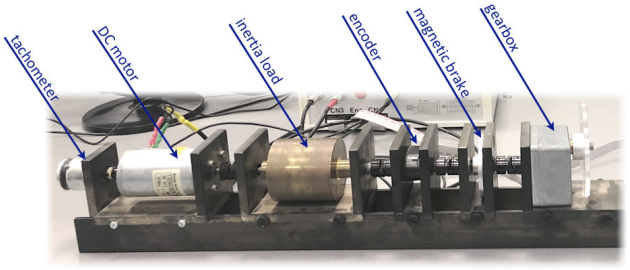

FIGURE 9. INTECO modular servo system.

PCI bus card and is interfaced with the MATLAB/Simulink environment. The system is presented in Fig. 9.

The input signal to the DC motor system is the voltage of the controlled voltage source, and the output is the angular velocity of the motor shaft. The system is modeled by a first-order transfer function, which in our case is identified as

$$G(s) = \frac{135.132}{0.875\,s + 1} \tag{41}$$

Similar models of this system have been considered in [41], [56], [59]. To perform the comparative analysis, we use implementations of the FOPID in terms of a) the time-invariant FIRBT-based model, b) the time-varying FIRBT-based model, c) discrete-time Oustaloup-based models, d) discrete-time modified Oustaloup-based models, e) the specific Oustaloup-based approach based on a classical PID controller and external filter (see subsection 5.3 in [41]), f) Tustin-CFE, and g) Euler-PSE-based models. The model (41) is controlled by FOPID controllers with parameters presented in Subsection IV-B. Step responses in terms of the output of the closed-loop system and control signals are presented in Fig. 10. Also, Fig. 10 shows errors in terms of differences of output and control signals between actual and approximate FOPID controllers.

It can be seen from Fig. 10 that the system output and control signal for the FIRBT, Euler-PSE-based models and the actual FOPID controller are hardly distinguishable from each other. The Oustaloup-based model and the time-varying FIRBT-based FOPID controllers also give satisfactory results. Slightly worse performances are obtained by both the Oustaloup-based controller and the specific FOPID model introduced in [41]. Tustin-CFE-based FIRBT model gives unsatisfactory accuracy in both transient and steady-state cases. Table. 3 depicts the L_2 norm of differences between output step responses for $t \in [0, 10]$ s of actual and approximate FOPID controllers for various modeling orders.

Considering the results in Table 3, we can notice that the high-frequency performance of the introduced methodology leads to a good modeling performance in closed-loop control. Again, we can see that in the case of the time-varying FIRBT-based model, to obtain similar effectiveness, we have to use higher model's orders as compared to the time-invariant FIRBT-based case.

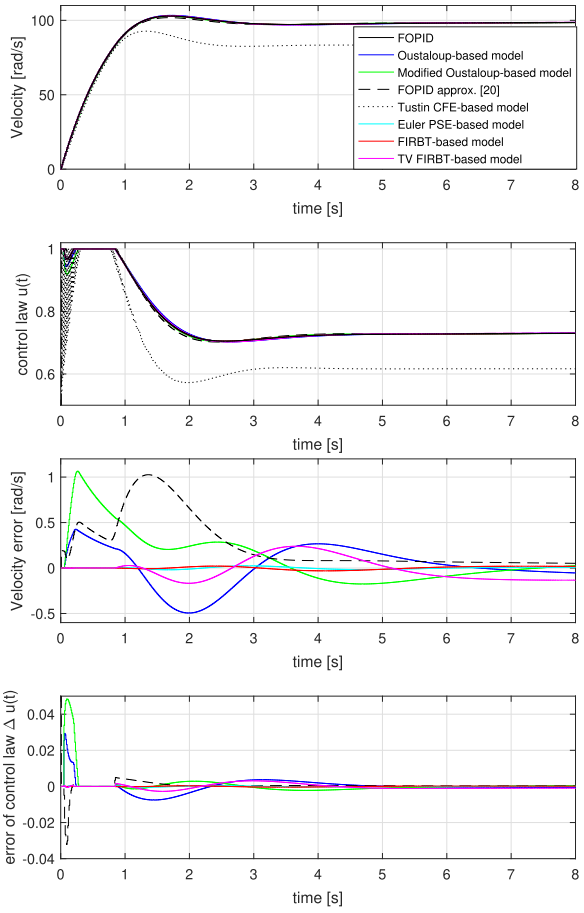

FIGURE 10. Output and control signals of the closed loop system (up) and errors (down) for various FOPID models.

It can also be seen from Table 3 that the Oustaloup-based approaches generate significantly greater errors. Moreover, increasing the orders $k_{PID} > 11$ for the both Oustaloup-based approaches does not increase the FOPID modeling performance in closed-loop control. It is due to the low approximation accuracy of the model for high frequencies, which is crucial in the closed-loop control. Note that, in the case of specific Oustaloup-based FOPID model considered in [41] the approximation errors are slightly higher than Oustaloup-based approaches.

The same experiments have been performed in real-life hardware. Step responses in terms of the output of the closed-loop system and control signals as well as errors in terms of differences of output and control signals between actual and approximate FOPID controllers are presented in Fig. 11.

It can be observed in Fig. 11 that the results are very similar to those presented in the simulation experiments. Again, the results for the actual FOPID controller, the FIRBT and Euler-PSE-based models are hardly distinguishable. Once again, Tustin-CFE-based FOPID produces the highest errors both in transient and steady states. The only difference as compared to the simulation experiments is the high-frequency noises generated by the encoder.

TABLE 3. L_2 norm of differences between output step responses of actual and approximate FOPID controllers.

Order	Oustaloup	Modified Oustaloup	FOPID approx. [41]	Tustin CFE	Euler PSE	FIRBT	TV FIRBT
$k_{PID} = 7$	12.1799	–	42.9306	566.0625	1.7889	3.8915	19.6487
$k_{PID} = 11$	6.2883	8.5171	14.8186	382.1995	0.3166	0.4603	3.4590
$k_{PID} = 15$	4.0083	7.6549	10.9416	260.1709	0.2156	0.2602	1.1500
$k_{PID} = 19$	4.3559	7.7220	10.7243	182.6543	0.3332	0.2155	0.6713
$k_{PID} = 23$	4.2148	7.7227	10.7674	132.6775	0.2191	0.2050	0.3210

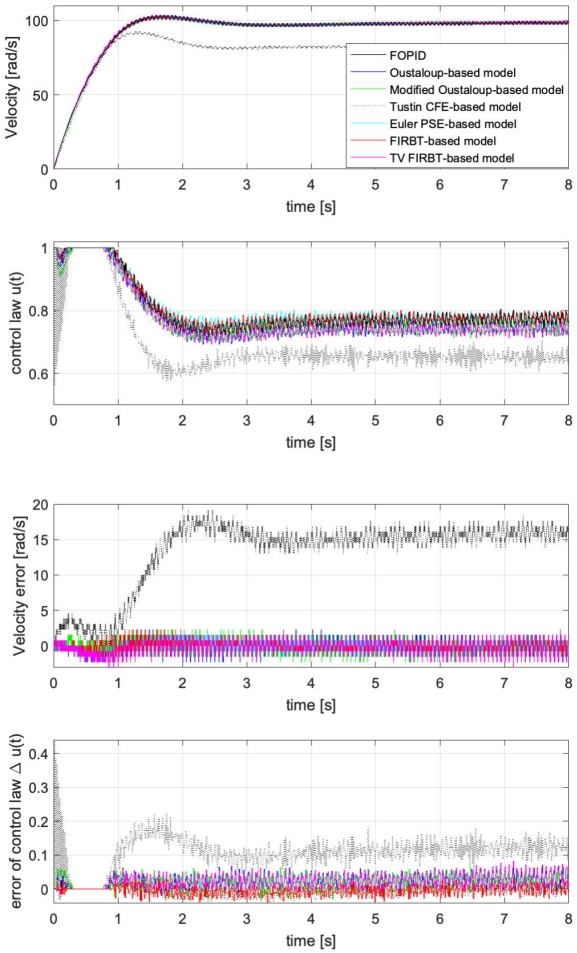

FIGURE 11. Output and control signals of the closed loop system (up) and errors (down) for various FOPID models.

In conclusion, the simulations and experiments presented above have proved that the methodology introduced in this paper can be effectively used for implementation of FOPID controllers. The introduced approach is computationally simple, contrary to the Euler-PSE-based model, and can be easily employed in the industrial environment.

VI. CONCLUSION

The paper has presented a new method of approximation of the discrete-time fractional-order PID controller. The approach is based on a specific representation of the FOPID controller, where fractional properties are modeled by the FIR-based filter, leading to the high FOPID modeling accuracy in the high-frequency range. In order to obtain an effective and low order model of FOPID controller, BT model order reduction using analytical solutions of the controllability and observability gramians is applied in the proposed approach. The Euler-PSE approximation gives comparable results to our FIRBT-based approach; however, in contrast to the FIRBT method, reducing the model is time-consuming due to the necessity of solving the Lyapunov equations. Also, the paper proposes the modification of the approximation methodology in terms of time-varying gains of the FOPID controller. In both cases, we obtain a low-order state-space model of the FOPID controller, which can be easily implemented in real-time applications on industrial computers of relatively low performance. Comparative analysis with various approaches confirms the efficiency of the introduced methodology to the implementation of the discrete-time FOPID controllers, which is also confirmed by the real-life experiment in terms of control of the DC motor servo system. A Matlab/Simulink implementation tool is provided as an appendix to the paper.

TABLE 4. Implementation methods in the Matlab/Simulink environment.

Method	Description
FIRbasedFOPID.m	FIR-based state-space model of the FOPID controller as in Eqs. (19)-(23)
FIRbasedFD.m	FIR-based state-space model of fractional-order difference
FIRbasedFI.m	FIR-based model of the fractional-order integrator
FIRBTbasedFOPID.m	Reduced order state space approximator of the FOPID controller as in Eqs. (30)-(33)
FIRbasedTVFOPID.m	Reduced order state space approximator of the FOPID controller with time varying gains as in Eqs. (37)-(40)
FIRBTbasedFD.m	Reduced order state space approximator of fractional-order difference
FIRBTbasedFI.m	Reduced order state space approximator of fractional-order integrator
BTbasedFOPID.slx	Blockset in the Matlab/Simulink environment of BT-based models of fractional-order difference, fractional-order integrator, and FOPID controllers
exampleFOPID.slx	Example of the FOPID-based closed-loop control of the DC motor model as in Section V
exampleFOPI.slx	Example of the FOPI-based closed-loop control of the DC motor model

APPENDIX
IMPLEMENTATION TOOL FOR MATLAB/SIMULINK

Implementation tool for FOPID controller in the Matlab/Simulink environment can be downloaded from [60]. The list of the methods of the tool is presented in Table 4.

REFERENCES

[1] I. Podlubny, "Fractional-order systems and $PI^{\lambda}D^{\mu}$ controllers," *IEEE Trans. Autom. Control*, vol. 44, no. 1, pp. 208–214, Jan. 1999.
[2] H. Ramezanian and S. Balochian, "Optimal design a fractional-order PID controller using particle swarm optimization algorithm," *Int. J. Control Automat.*, vol. 6, no. 4, pp. 55–67, 2013.
[3] S. Momani, R. El-Khazali, and I. M. Batiha, "Tuning PID and $PI^{\lambda}D^{\delta}$ controllers using particle swarm optimization algorithm via El-Khazali's approach," in *Proc. AIP Conf.*, vol. 2172, no. 1, Nov. 2019, Art. no. 050003.
[4] Z. Gao and X. Liao, "Improved oustaloup approximation of fractional-order operators using adaptive chaotic particle swarm optimization," *J. Syst. Eng. Electron.*, vol. 23, no. 1, pp. 145–153, Feb. 2012.
[5] I. Pan, S. Das, and A. Gupta, "Handling packet dropouts and random delays for unstable delayed processes in NCS by optimal tuning of $PI^{\lambda}D^{\delta}$ controllers with evolutionary algorithms," *ISA Trans*, vol. 50, no. 4, pp. 557–572, 2011.
[6] H. P. Ren and T. Zheng, "Optimization design of power factor correction converter based on genetic algorithm," in *Proc. 4th Int. Conf. Genetic Evol. Comput.*, Dec. 2010, pp. 293–296.
[7] M. A. Ravari and M. Yaghoobi, "Optimum design of fractional order PID controller using chaotic firefly algorithms for a control CSTR system," *Asian J. Control*, vol. 21, no. 5, pp. 2245–2255, 2019.
[8] I. Birs, C. Muresan, I. Nascu, and C. Ionescu, "A survey of recent advances in fractional order control for time delay systems," *IEEE Access*, vol. 7, pp. 30951–30965, 2019.
[9] A. S. Bazanella, L. F. A. Pereira, and Ad. Parraga, "A new method for PID tuning including plants without ultimate frequency," *IEEE Trans. Control Syst. Technol.*, vol. 25, no. 2, pp. 637–644, May 2017.
[10] J. Muñoz, C. A. Monje, L. F. Nagua, and C. Balaguer, "A graphical tuning method for fractional order controllers based on iso-slope phase curves," *ISA Trans.*, vol. 105, pp. 296–307, Oct. 2020.
[11] S. K. Verma, S. Yadav, and S. K. Nagar, "Optimization of fractional order PID controller using grey wolf optimizer," *J. Control Autom. Electr. Syst.*, vol. 28, no. 3, pp. 314–322, 2017.
[12] F. Meng, S. Liu, and K. Liu, "Design of an optimal fractional order PID for constant tension control system," *IEEE Access*, vol. 8, pp. 58933–58939, 2020.
[13] F. Zhang, C. Yang, X. Zhou, and W. Gui, "Optimal setting and control strategy for industrial process based on discrete-time fractional-order $PI^{\lambda}D^{\mu}$," *IEEE Access*, vol. 7, pp. 47747–47761, 2019.
[14] M. Yaghi and E. M. Önder, "H_2/H_∞-neural-based FOPID controller applied for radar-guided missile," *EEE Trans. Ind. Electron.*, vol. 67, no. 6, pp. 4806–4814, Jul. 2020.
[15] F. Meng, S. Liu, A. Pang, and K. Liu, "Fractional order PID parameter tuning for solar collector system based on frequency domain analysis," *IEEE Access*, vol. 8, pp. 148980–148988, 2020.
[16] A. Dumlu and K. Erenturk, "Trajectory tracking control for a 3-DOF parallel manipulator using fractional-order $PI^{\lambda}D^{\mu}$ control," *IEEE Trans. Ind. Electron.*, vol. 61, no. 7, pp. 3417–3426, Aug. 2014.
[17] K. Bettou and A. Charef, "Control quality enhancement using fractional $PI^{\lambda}D^{\mu}$ controller," *Int. J. Syst. Sci.*, vol. 40, no. 8, pp. 88–875, 2009.
[18] H. Ren, J. Fan, and O. Kaynak, "Optimal design of a fractional-order proportional-integer-differential controller for a pneumatic position servo system," *IEEE Trans. Ind. Electron.*, vol. 66, no. 8, pp. 6220–6229, Sep. 2019.
[19] A. Mughees and S. A. Mohsin, "Design and control of magnetic levitation system by optimizing fractional order PID controller using ant colony optimization algorithm," *IEEE Access*, vol. 8, pp. 116704–116723, 2020.
[20] P. Shah and S. Agashe, "Review of fractional PID controller," *Mechatronics*, vol. 38, pp. 29–41, Sep. 2016.
[21] S. W. Seo and H. H. Choi, "Digital implementation of fractional order PID-type controller for boost dc-dc converter," *IEEE Access*, vol. 7, pp. 142652–142662, 2019.
[22] J. Zhang, Z. Jin, Y. Zhao, Y. Tang, F. Liu, Y. Lu, and P. Liu, "Design and implementation of novel fractional-order controllers for stabilized platforms," *IEEE Access*, vol. 8, pp. 93133–93144, 2020.
[23] M. Zhou, Y. Yu, J. Zhang, and W. Gao, "Iterative learning and fractional order PID hybrid control for a piezoelectric micro-positioning platform," *IEEE Access*, vol. 8, pp. 144654–144664, 2020.
[24] W. Malesza, M. Macias, and D. Sierociuk, "Analytical solution of fractional variable order differential equations," *J. Comput. Appl. Math.*, vol. 348, pp. 214–236, Mar. 2019.
[25] M. D. Ortigueira, D. Valério, and J. T. Machado, "Variable order fractional systems," *Commun. Nonlinear Sci. Numer. Simul.*, vol. 71, pp. 231–243, Jun. 2019.
[26] P. Oziablo, D. Mozyrska, and M. Wyrwas, "Discrete-time fractional, variable-order PID controller for a plant with delay," *Entropy*, vol. 22, no. 7, p. 771, Jul. 2020.
[27] D. Sierociuk and M. Macias, "Comparison of variable fractional order PID controller for different types of variable order derivatives," in *Proc. 14th Int. Carpathian Control Conf. (ICCC)*, May 2013, pp. 9–334.
[28] D. Sierociuk and M. S. Wiraszka, "Variable-order PI control algorithm with order scheduled according to the control error and anti-windup strategy," in *Proc. 20th Int. Carpathian Control Conf. (ICCC)*, May 2019, pp. 1–5.
[29] D. Sierociuk and M. S. Wiraszka, "A new variable fractional-order PI algorithm," *IFAC Papers OnLine*, vol. 51, no. 4, pp. 745–750, 2018.
[30] C. A. Monje, Y. Q. Chen, B. M. Vinagre, D. Xue, and V. Feliu-Batlle, *Fractional-order Systems and Controls: Fundamentals and Applications* (Series on Advances in Industrial Control). London, U.K.: Springer-Verlag, 2020.
[31] B. M. Vinagre, I. Podlubny, A. Hernandez, and V. Feliu, "Some approximations of fractional order operators used in control theory and applications," *Fractional Calculus Appl. Anal.*, vol. 3, no. 3, p. 945, 2000.
[32] Z. Li, L. Liu, S. Dehghan, Y. Q. Chen, and D. Xue, "A review and evaluation of numerical tools for fractional calculus and fractional order controls," *Int. J. Control*, vol. 90, no. 6, pp. 1165–1181, 2017.
[33] Q. Zhang, B. Song, H. Zhao, and J. Zhang, "Discretization of fractional order differentiator and integrator with different fractional orders," *Intell. Control Autom.*, vol. 8, no. 2, pp. 75–85, 2017.
[34] R. El-Khazali, "Fractional-order $PI^{\lambda}D^{\mu}$ controller design," *Comput. Math. Appl.*, vol. 66, no. 5, p. 639, 2013.
[35] R. Stanisławski, K. J. Latawiec, and M. Lukaniszyn, "A comparative analysis of Laguerre-based approximators to the Grünwald–Letnikov fractional-order difference," *Math. Problems Eng.*, vol. 512104, pp. 1–10, Dec. 2015.
[36] T. Abdeljawad, "On Riemann and Caputo fractional differences," *Comput. Math. Appl.*, vol. 62, no. 3, pp. 1602–1611, Aug. 2011.
[37] R. Scherer, S. L. Kalla, Y. Tang, and J. Huang, "The Grünwald–Letnikov method for fractional differential equations," *Comput. Math. Appl.*, vol. 62, no. 3, pp. 902–917, 2011.
[38] R. Stanisławski and K. J. Latawiec, "A modified mikhailov stability criterion for a class of discrete-time noncommensurate fractional-order systems," *Commun. Nonlinear Sci. Numer. Simul.*, vol. 96, May 2021, Art. no. 105697.
[39] A. Tepljakov, E. Petlenkov, and J. Belikov. (2020). *FOMCON Toolbox; 2011*. [Online]. Available: http://www.fom con.net/
[40] A. Chevalier, C. Francis, C. Copot, C. M. Ionescu, and R. De Keyser, "Fractional-order PID design: Towards transition from state-of-art to state-of-use," *ISA Trans.*, vol. 84, pp. 178–186, Jan. 2019.
[41] A. Tepljakov, E. A. Gonzalez, E. Petlenkov, J. Belikov, C. A. Monje, and I. Petráš, "Incorporation of fractional-order dynamics into an existing PI/PID DC motor control loop," *ISA Trans.*, vol. 60, pp. 262–273, Jan. 2016.
[42] D. Xue, *Fractional-Order Control Systems: Fundamentals and Numerical Implementations*. Berlin, Germany: De Gruyter, 2017.
[43] D. Xue. (2020). *FOTF Toolbox; 2017*. [Online]. Available: https://www.mathworks.com/matlabcentral/fileexchange/60874-fotf-toolbox
[44] P. Oziablo, D. Mozyrska, and M. Wyrwas, "Discrete-time fractional, variable-order PID controller for a plant with delay," *Entropy*, vol. 22, no. 7, p. 771, 2020.
[45] R. Stanisławski, M. Rydel, and L. KJ, "New implementation of discrete-time fractional-order PI controller by use of model order reduction methods," in *Advanced, Contemporary Control. Advances in Intelligent Systems and Computing*. vol. 1196. Cham, Switzerland: Springer, 2020, pp. 209–1199.

[46] F. Merrikh-Bayat, S.-N. Mirebrahimi, and M. R. Khalili, "Discrete-time fractional-order PID controller: Definition, tuning, digital realization and some applications," *Int. J. Control Automat. Syst.*, vol. 13, no. 1, pp. 81–90, 2015.
[47] W. Krajewski and U. Viaro, "A method for the integer-order approximation of fractional-order systems," *J. Franklin Inst.*, vol. 351, no. 1, pp. 555–564, 2014.
[48] R. Stanisławski, M. Rydel, and K. J. Latawiec, "Modeling of discrete-time fractional-order state space systems using the balanced truncation method," *J. Franklin Inst.*, vol. 354, no. 7, pp. 3008–3020, 2017.
[49] J. Shen and J. Lam, "H_∞ model reduction for positive fractional order systems," *Asian J. Control*, vol. 16, no. 2, pp. 441–450, 2014.
[50] M. Rydel, "New integer-order approximations of discrete-time non-commensurate fractional-order systems using the cross Gramian," *Adv. Comput. Math.*, vol. 45, no. 2, pp. 631–653, 2019.
[51] (2020). INTECO LLC. *Modular Servo*. [Online]. Available: http://www.inteco.com.pl/products/modular-servo/
[52] S. Hilger, "Analysis on measure chains—A unified approach to continuous and discrete calculus," *Results Math.*, vol. 18, no. 1, pp. 18–56, 1990.
[53] M. D. Ortigueira and J. A. T. Machado, "New discrete-time fractional derivatives based on the bilinear transformation: Definitions and properties," *J. Adv. Res.*, vol. 25, pp. 1–10, Sep. 2020.
[54] T. Penzl, "Eigenvalue decay bounds for solutions of Lyapunov equations: The symmetric case," *Syst. Control Lett.*, vol. 40, no. 2, pp. 139–144, 2000.
[55] J. Sabatier, "Solutions to the sub-optimality and stability issues of recursive pole and zero distribution algorithms for the approximation of fractional order models," *Algorithms*, vol. 11, no. 7, p. 103, 2018.
[56] Inteco. *Modular Servo System User's Manual*. [Online]. Available: http://www.inteco.com.pl/Docs/Servo_um.pdf
[57] W. Bauer, J. Baranowski, S. Kapoulea, and C. Psychalinos, "Digital and analog design of fractional PD controller for a servo system," in *Proc. 24th Int. Conf. Methods Models Automat. Robot. (MMAR)*, Aug. 2019, pp. 7–472.
[58] I. Dimeas, I. Petras, and C. Psychalinos, "New analog implementation technique for fractional-order controller: A DC motor control," *AEU-Int. J. Electron. Commun.*, vol. 78, pp. 192–200, Aug. 2017.
[59] S. Kapoulea, C. Psychalinos, J. Baranowski, and W. Bauer, "CCII based realization of fractional-order PD controller for a position servo," in *Proc. 42nd Int. Conf. Telecommun. Signal Process. (TSP)*, Jul. 2019, pp. 5–102.
[60] R. Stanislawski, M. Rydel, and Z. Li. (2022). *FOPID Tool*. Accessed: 2022. [Online]. Available: http://doi.org/10.5281/zenodo.6009533

RAFAŁ STANISŁAWSKI received the M.Sc. and Ph.D. degrees in electrical engineering and the Habilitation degree in control and robotics from the Department of Electrical, Control and Computer Engineering, Opole University of Technology, Opole, Poland, in 2000, 2005, and 2014, respectively. He is currently an Associate Professor and the Head of the Department's Group of Computer-Controlled Systems. His research interests include modeling and analysis and control of dynamic systems, in particular fractional-order systems.

MAREK RYDEL received the M.Sc. degree in electronic engineering from the Wrocław University of Science and Technology, in 2002, and the Ph.D. and Habilitation degrees in control and robotics from the Opole University of Technology, in 2009 and 2020, respectively. He is currently an Associate Professor with the Department of Electrical, Control and Computer Engineering, Opole University of Technology, Poland. His research interests include model order reduction of large scale dynamical systems, including fractional-order systems.

ZHIXIONG LI (Senior Member, IEEE) received the Ph.D. degree in transportation engineering from the Wuhan University of Technology, in 2013. He is currently with the Faculty of Mechanical Engineering, Opole University of Technology, Opole, Poland, and the Director of the International Joint Research Centre on Renewable Energy and Sustainable Marine Vehicles. He has authored/coauthored two books and over 100 articles. His research interests include dynamic system modeling and optimization and machine learning and applications. He is an Associate Editor of IEEE TRANSACTION ON INTELLIGENT TRANSPORTATION SYSTEMS and a Column Editor of *IEEE Intelligent Transportation Systems Magazine*.